Title

Interface Model for Bond-Slip and Dowel-Action Behavior

Journal

ACI STRUCTURAL JOURNAL, 114(4)

ISSN

0889-3241

Authors

Kottari, Alexandra

Mavros, Marios

Murcia-Delso, Juan

et al.

Publication Date

2017

DOI

10.14359/51689870

Peer reviewed

ACI STRUCTURAL JOURNAL TECHNICAL PAPER

Title No. 114-S85

Interface Model for Bond-Slip and Dowel-Action Behavior

by Alexandra Kottari, Marios Mavros, Juan Murcia-Delso, and P. Benson Shing

This paper presents an interface element formulation for modeling dowel action and bond-slip behavior of steel reinforcing bars in the finite element analysis of concrete structures. The interface connects steel bar elements to concrete elements, and allows bar elements to have a smaller size than the concrete elements to which they are connected, to improve computational efficiency as well as flexibility in meshing. It adopts a cyclic bond stress-versus-slip law developed by the last two authors, and extends a dowel-action model developed for monotonic loading to cyclic loading. A numerical study has been conducted to demonstrate the benefits of using a bond-slip model in eliminating the mesh-size dependency of numerical results that can otherwise be introduced by bar elements directly connected to concrete elements and the accuracy and computational efficiency provided by the proposed interface formulation. The capability of the model to simulate dowel action has been validated with results from monotonic and cyclic shear loading tests performed on individual dowel bars, as well as shear keys in bridge abutments.

Keywords: bond slip; dowel action; interface element; reinforced concrete; shear keys.

INTRODUCTION

The behavior of reinforced concrete structures can be significantly affected by the bond slip and dowel action of the reinforcing steel, which normally occur in the vicinity of a crack. To accurately simulate the bond-slip and dowel-action phenomena using nonlinear finite element models, high-fidelity constitutive relations for the concrete, steel, and their contact are needed. Moreover, the length of the steel bar elements has to be sufficiently small to adequately capture the variation of the contact stresses between the bar and the surrounding concrete over a distance that can be three to four times the bar diameter. The use of a sufficiently fine mesh for such analysis is often impractical in the modeling of reinforced concrete structures.

Dowel action involves the flexural deformation of the bar and the compressive deformation of the concrete in contact. Hence, the dowel resistance developed is governed by the compressive strength of the concrete, which can be significantly higher than the uniaxial compressive strength due to the confinement effect of the surrounding concrete. To model the dowel action accurately, a three-dimensional (3-D) constitutive model that can account for the increased compressive strength of confined concrete is needed. However, a 3-D finite element model with a fine mesh can be computationally prohibitive.

To efficiently and accurately model the bond-slip behavior of reinforcing steel in finite element analysis, the nonlinear behavior of concrete during bar slip can be represented in zero-thickness interface elements connecting the reinforcing steel to the concrete (for example, refer to Cox and Herrmann [1998] and Murcia-Delso and Shing [2015]). In this study, this approach has been extended to model dowel action in addition to bond slip with a two-dimensional (2-D) interface element. For this purpose, a cyclic constitutive law has been introduced to model the dowel resistance in the normal direction of the interface, while the phenomenological cyclic bond-slip law proposed by Murcia-Delso and Shing (2015) has been adopted in the tangential direction. To improve the computational efficiency, a new interface element formulation is presented for connecting reinforcing bar elements to concrete elements, whereby the reinforcing bars can be represented by a fine mesh while the concrete by a much coarser mesh. This ensures that high-resolution interfacial stress distributions can be obtained while avoiding having concrete elements smaller than the minimum representative volume for which concrete can be considered a homogenous material. It is generally accepted that the minimum representative volume of concrete is at least three to five times the maximum aggregate size (Van Mier and Van Vliet 2003).

Numerous models have been proposed for the calculation of dowel resistance. Soroushian et al. (1987) has shown that the secant bearing stiffness of concrete during dowel action is proportional to the square root of its uniaxial compressive strength and is inversely proportional to the bar diameter. The confinement effect can significantly increase the bearing strength of concrete. Dulacska (1972) and Vintzeleou and Tassios (1987) have suggested that the bearing strength of concrete under dowel action can be taken to be four times the uniaxial compressive strength. However, Dei Poli et al. (1992) have demonstrated that the bearing stiffness of concrete is not constant, but a nonlinear function of the dowel force. In this study, the formula proposed by Brenna et al. (1990) to calculate the bearing stiffness of concrete under the monotonic loading condition has been extended for cyclic loading and implemented in the interface model.

In this paper, the new element formulation and the cyclic dowel-action law are presented, the bond-slip law of Murcia-Delso and Shing (2015) is concisely summarized, and the accuracy and computational efficiency provided by the new element are demonstrated. The accuracy of the dowel-action model is validated by experimental results.

ACI Structural Journal, V. 114, No. 4, July-August 2017.
MS No. S-2016-351.R1, doi: 10.14359/51689870, received October 19, 2016, and reviewed under Institute publication policies.

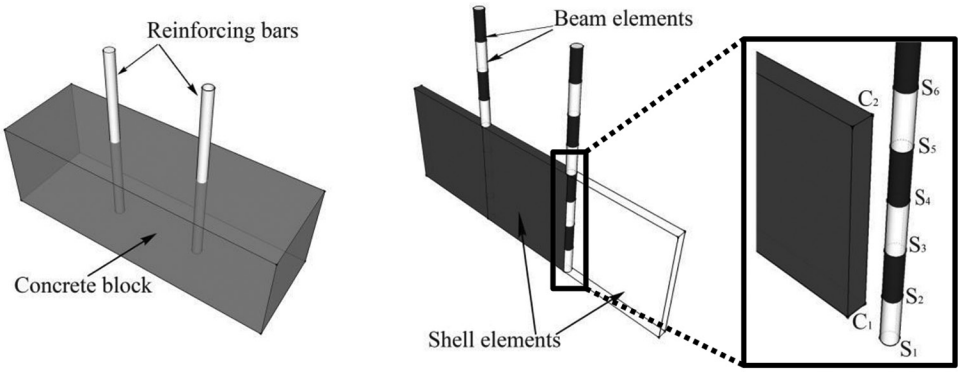

Fig. 1—Modeling of bar-concrete interaction: (a) physical model; (b) FEA model; and (c) element size mismatch.

RESEARCH SIGNIFICANCE

The bond slip and dowel action of reinforcing bars have an important influence on the inelastic behavior of reinforced concrete structures. A new interface element formulation is presented in this paper for the modeling of these phenomena in an accurate and efficient manner. The element simulates the bond-slip and dowel-action phenomena in a zero-thickness interface between the reinforcing bar and the surrounding concrete using appropriate constitutive models that account for the damage of concrete induced by these actions. The main novelty of the element is that it allows the reinforcing bar to be represented by a sufficiently fine mesh needed to model these phenomena accurately, and the concrete by a much coarser mesh. This can significantly improve computational efficiency and make such analysis practical.

MODEL FORMULATION

Element formulation

To simulate the phenomena of bond slip and dowel action in a finite element model, reinforcing bars normally require a relatively fine mesh to accurately capture the variation of the shear and normal stresses along the bar-concrete interface, as compared to the size of concrete elements needed to capture the nonlinear behavior of a reinforced concrete member. In this situation, it is computationally more efficient to have different element sizes for the bars and the concrete, which are connected via interface elements that account for the bond slip and dowel action. Figure 1 illustrates an example in which four bar elements are connected to a single concrete element. For this purpose, a specially formulated four-node, zero-thickness interface element is proposed to connect each of these bars to the concrete element and represent appropriate contributions to the bond and dowel forces, as illustrated in Fig. 2.

Figure 3 shows the configuration of an isolated interface element with Gauss points G_1 and G_2. It is intended for four-node planar concrete elements. Nodes 3 and 4 are connected to the concrete element, while Nodes 1 and 2 are connected to the bar element. It is so formulated that the length of the bar element (L_{12}) has to be equal to, or shorter than, the length of the concrete element (L_{34}), and that the bar element (that is, Nodes 1 and 2) has to be located between Nodes 3

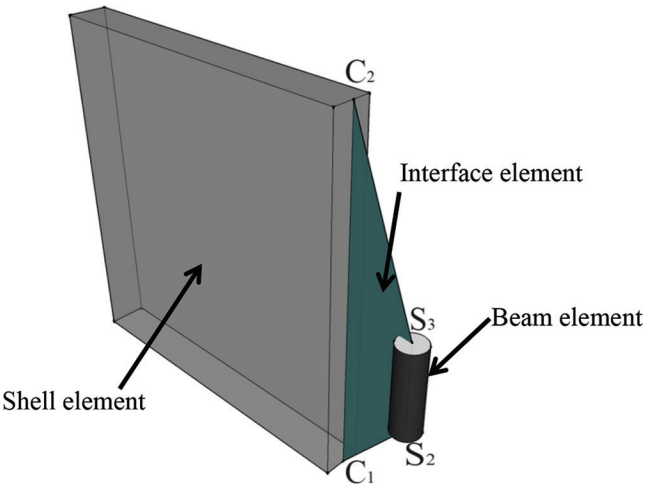

Fig. 2—Bar-concrete connectivity through interface element.

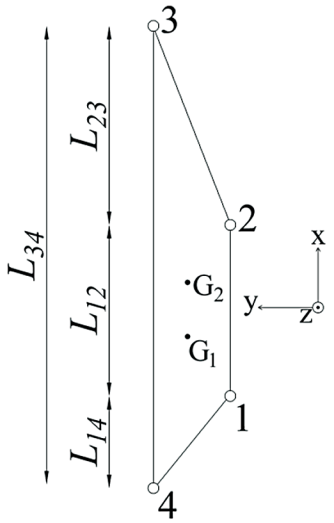

Fig. 3—Interface element.

and 4 in the undeformed state. The local coordinate x has its origin at the midpoint between Nodes 1 and 2. Each node i of the interface element has two degrees of freedom—that is, displacements in the x- and y-directions, denoted by u_i and v_i, respectively. The shear (bond) stress τ and the normal (dowel) stress σ along the element depend on the values and

histories of the relative tangential displacement (slip) $\tilde{u}$ and relative normal displacement $\tilde{v}$, which are defined as

$$\begin{Bmatrix} \tilde{u} \\ \tilde{v} \end{Bmatrix} = \begin{Bmatrix} u_s(x) - u_c(x) \\ v_s(x) - v_c(x) \end{Bmatrix} \quad (1)$$

in which u and v are the displacements in the x- and y-directions, determined by the displacement shape functions and the nodal displacements. Subscripts c and s denote the displacements at the concrete side and the bar side of the element, respectively. To account for the different lengths, the bar side (1-2) and the concrete side (3-4) have their individual natural coordinates η and η_c, respectively, which are mapped to the x-coordinate as follows: $x = (L_{12}/2) \cdot \eta$ and $x = (L_{23} - L_{14})/2 + (L_{34}/2) \cdot \eta_c$. Hence, coordinates η and η_c have the following linear relation

$$\eta_c = \alpha + \beta \cdot \eta \quad (2)$$

where

$$\alpha = \frac{L_{14} - L_{23}}{L_{34}} \quad (3)$$

$$\beta = \frac{L_{12}}{L_{34}} \quad (4)$$

The displacements of any point along the bar side are given by

$$u_s(\eta) = N_1(\eta) \cdot u_1 + N_2(\eta) \cdot u_2 \quad (5)$$

$$v_s(\eta) = N_1(\eta) \cdot v_1 + N_2(\eta) \cdot v_2 \quad (6)$$

in which N_i is linear shape functions defined in natural coordinate η as follows

$$N_1(\eta) = \frac{1 - \eta}{2} \quad (7)$$

$$N_2(\eta) = \frac{1 + \eta}{2} \quad (8)$$

The displacements along the concrete side are defined in the same way as follows

$$u_c(\eta_c) = N_1(\eta_c) \cdot u_4 + N_2(\eta_c) \cdot u_3 \quad (9)$$

$$v_c(\eta_c) = N_1(\eta_c) \cdot v_4 + N_2(\eta_c) \cdot v_3 \quad (10)$$

Based on the relation in Eq. (2), the relative displacements along the interface can be expressed as functions of η.

$$\begin{Bmatrix} \tilde{u} \\ \tilde{v} \end{Bmatrix} = \begin{Bmatrix} u_s(\eta) - u_c(\alpha + \beta \cdot \eta) \\ v_s(\eta) - v_c(\alpha + \beta \cdot \eta) \end{Bmatrix} = \begin{bmatrix} \mathbf{b}(\eta) & \mathbf{0} \\ \mathbf{0} & \mathbf{b}(\eta) \end{bmatrix} \cdot \begin{Bmatrix} \mathbf{u} \\ \mathbf{v} \end{Bmatrix} \quad (11)$$

where

$$\mathbf{b}(\eta) = [N_1(\eta) \quad N_2(\eta) \quad -N_2(\alpha + \beta \cdot \eta) \quad N_1(\alpha + \beta \cdot \eta)] \quad (12)$$

and

$$\begin{Bmatrix} \mathbf{u} \\ \mathbf{v} \end{Bmatrix} = \begin{bmatrix} u_1 & u_2 & u_3 & u_4 & v_1 & v_2 & v_3 & v_4 \end{bmatrix}^T \quad (13)$$

With $\tilde{u}$ and $\tilde{v}$ given by Eq. (11), the values of the shear and normal stresses τ and σ are determined by a set of constitutive laws. As described in the following two sections, the stress-strain relations in the normal and tangential directions are assumed to be independent for the sake of simplicity. Each concrete element is in contact with one or more bar elements. Hence, for each interface element, only the stresses along the length of the connected bar element (that is, L_{12} as shown in Fig. 3) are determined and used to calculate the element nodal forces. For a unit length of the steel bar with diameter d_b, the shear stress τ acts around the bar circumference πd_b, while the normal stress σ is assumed to act on a rectangular area d_b, which represents the projection of the contact surface between the bar and the concrete on the x-z plane. The element forces can be formulated with the principle of virtual displacements, with the internal virtual work given by

$$\delta W_I = -\pi d_b \int_0^{L_{12}} \delta\tilde{u} \cdot \tau dx - d_b \int_0^{L_{12}} \delta\tilde{v} \cdot \sigma dx \quad (14)$$

and the external virtual work by

$$\delta W_E = \delta\mathbf{u}^T \mathbf{F}_x + \delta\mathbf{v}^T \mathbf{F}_y \quad (15)$$

in which $\delta\tilde{u}$ and $\delta\tilde{v}$ are the virtual relative displacements along the element; $\delta\mathbf{u}$ and $\delta\mathbf{v}$ are the vectors of virtual nodal displacements; and $\mathbf{F}_x$ and $\mathbf{F}_y$ are vectors of element nodal forces in the x- and y-directions. With Eq. (11), (14), and (15) and the principle of virtual displacements, $\delta W_I + \delta W_E = 0$, one has

$$\begin{aligned} \mathbf{F}_x &= \pi \cdot d_b \cdot \int_{-1}^{1} \mathbf{b}(\eta)^T \cdot \tau(\eta) \cdot J d\eta \\ \mathbf{F}_y &= d_b \cdot \int_{-1}^{1} \mathbf{b}(\eta)^T \cdot \sigma(\eta) \cdot J d\eta \end{aligned} \quad (16)$$

where

$$J = \frac{dx}{d\eta} = \frac{L_{12}}{2} \quad (17)$$

Constitutive law for bond-slip behavior

The bond-slip law proposed by Murcia-Delso and Shing (2015) has been adopted herein to describe the stress-displacement relation in the tangential direction of the interface element. However, the interaction with the displacements in the normal direction proposed in the original law has been ignored for simplicity. The model accounts for the bond-strength degradation caused by bar slip, cyclic slip reversals, and the tensile yield of a bar.

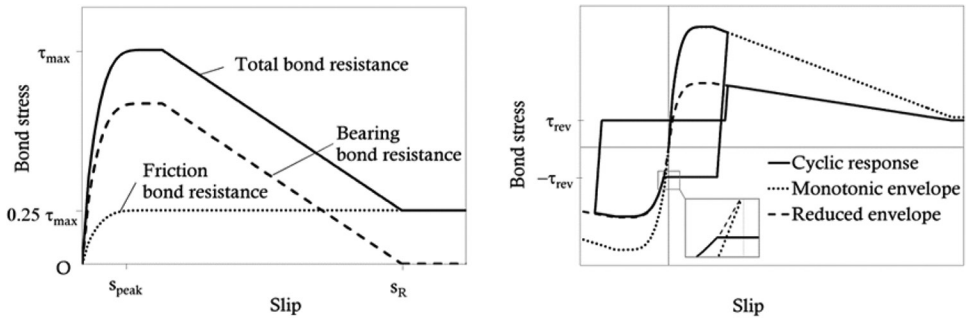

Fig. 4—Bond-slip model: (a) monotonic response; and (b) cyclic response (Murcia-Delso and Shing 2015).

Figure 4 shows the bond stress-slip relations for monotonic and cycle loading. In the model, the bond resistance is assumed to be provided by two mechanisms: the bearing force on the bar ribs due to mechanical interlock, and the friction force between the concrete and bar surfaces. Chemical adhesion between the concrete and the reinforcing bars is not modeled, as it is lost at relatively low bond stresses (Fédération Internationale du Béton 2000). However, its contribution to the initial bond resistance is implicitly considered in the bond-slip curves, which were calibrated with experimental data. The monotonic bond-slip envelope curve is given by Eq. (18), (19) and (20)

$$\tau = \rho_{b,s} \cdot \rho_{b,c} \cdot \tau_b + \rho_{f,s} \cdot \rho_{f,c} \cdot \tau_f \tag{18}$$

where

$$\tau_b(\tilde{u}) = \begin{cases} 3.0\dfrac{\tau_{\max}}{s_{peak}}\tilde{u} & \text{for } 0 \le \tilde{u} < 0.1 s_{peak} \\ \text{sign}(\tilde{u}) \cdot \tau_{max}\left[0.75 - 0.45\left(\dfrac{|\tilde{u}| - s_{peak}}{0.9 s_{peak}}\right)^4\right] & \text{for } 0.1 s_{peak} \le |\tilde{u}| < s_{peak} \\ \text{sign}(\tilde{u}) \cdot 0.75\tau_{\max} & \text{for } s_{peak} \le |\tilde{u}| < 1.1 s_{peak} \\ \text{sign}(\tilde{u}) \cdot 0.75\tau_{max}\left[1 - \dfrac{|\tilde{u}| - 1.1 s_{peak}}{s_R - 1.1 s_{peak}}\right] & \text{for } 1.1 s_{peak} \le |\tilde{u}| < s_R \\ 0 & \text{for } |\tilde{u}| \ge s_R \end{cases} \tag{19}$$

and

$$\tau_f(\tilde{u}) = \begin{cases} \dfrac{\tau_{max}}{s_{peak}}\tilde{u} & \text{for } 0 \le |\tilde{u}| < 0.1 s_{peak} \\ \text{sign}(\tilde{u}) \cdot \tau_{max}\left[0.25 - 0.15\left(\dfrac{\tilde{u} - s_{peak}}{0.9 s_{peak}}\right)^4\right] & \text{for } 0.1 s_{peak} \le |\tilde{u}| < s_{peak} \\ \text{sign}(\tilde{u}) \cdot 0.25\tau_{max} & \text{for } |\tilde{u}| \ge s_{peak} \end{cases} \tag{20}$$

in which τ_b is the bond resistance due to bearing action; τ_f is the frictional bond resistance; τ_{max} and τ_{res} are the maximum and residual bond strengths for monotonic loading; s_{peak} is the slip at which the peak strength is attained; s_R is the clear spacing between the bar ribs; $\rho_{b,s}$ and $\rho_{f,s}$ account for the reduction of the bearing (τ_b) and friction (τ_f) resistances due to the tensile yielding of the bar; and $\rho_{b,c}$ and $\rho_{f,c}$ account for the strength degradation due to cyclic slip reversals. Expressions for the strength reduction factors as well as the cyclic loading and unloading rules can be found in Murcia-Delso and Shing (2015).

The bond-slip law requires the calibration of only three parameters: τ_{max}, s_{peak}, and s_R. As suggested by Murcia-Delso and Shing (2015), the values for these parameters can be determined with the following empirical relations.

$$\tau_{\max} = 2.4 \cdot \left(\frac{f_c'}{5.0}\right)^{0.75} \tag{21}$$

$$s_{peak} = 0.07 \cdot d_b \tag{22}$$

$$s_R = 0.5 \cdot d_b \tag{23}$$

in which d_b is the bar diameter, in in.; f_c' is the concrete compressive strength, in ksi; and τ_{max} is in ksi.

Constitutive law for dowel action

The empirical formulation proposed by Brenna et al. (1990) to model the dowel action of a reinforcing bar under monotonic loading, as shown in Eq. (24) and (25), has been adopted to establish the compressive normal stress-displacement relation for the interface. The model is based on the test data of Soroushian et al. (1987) and is formulated as follows

$$\sigma(\tilde{v}) = \omega(\tilde{v}) \cdot k_0 \cdot \tilde{v} \tag{24}$$

in which

$$\begin{aligned} k_0 &= 370.25 \cdot f_c'^{0.75}/d_b \\ \omega(\tilde{v}) &= \left[1.5 \cdot \left(a + \sqrt{d^2 \cdot (40 \cdot \tilde{v}/d_b - b)^2 + c^2}\right)\right]^{-4/3} \\ a &= 0.59 - 0.07586 \cdot f_c' \\ b &= 0.0517 \cdot f_c' - 0.23 \\ c &= 0.0262 \cdot f_c' + 0.44 \\ d &= 0.0172 \cdot f_c' + 0.58 \end{aligned} \tag{25}$$

In the previous equations, f_c' is the concrete compressive strength; d_b is the bar diameter, $\tilde{v}$ is the imposed compres-

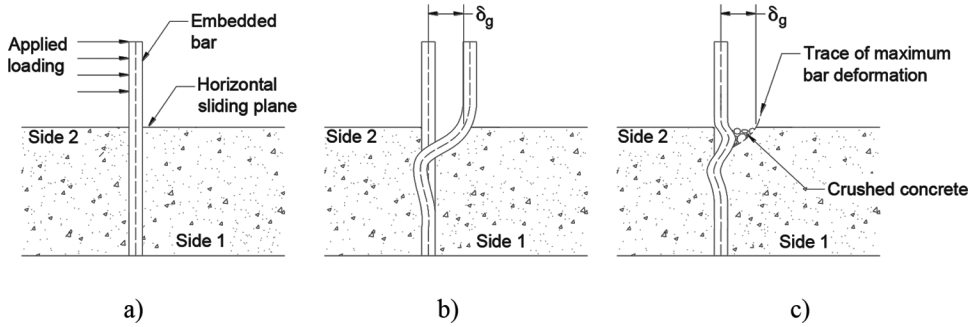

Fig. 5—Damage of concrete during dowel action: (a) physical problem; (b) loading; and (c) unloading.

sive displacement, and σ is the normal compressive stress. All units are in ksi and inches.

In this study, the dowel-action law presented herein has been extended for cyclic loading. Consider that the reinforcing bar is embedded in a concrete block, as shown in Fig. 5(a). The cyclic behavior is divided into three regimes. First, consider that the reinforcing bar deforms in flexure toward Side 1, as shown in Fig. 5(b). The concrete in the vicinity of the bar on Side 1 experiences compression and can be severely damaged. However, due to the confinement provided by the surrounding concrete, the compressive strength of the concrete in contact with the bar is significantly higher than that under uniaxial compression, and the increased compressive resistance is accounted for in Eq. (24) and (25).

Once the imposed displacement is reversed, the bar loses contact with concrete on Side 1 and the compressive stress on the bar diminishes. The decrease in stress is calculated as elastic unloading

$$\dot{\sigma}(\tilde{v}) = K_{un} \cdot \dot{\tilde{v}} \qquad K_{un} = \gamma \cdot K_{in} \tag{26}$$

in which the superposed dot represents the rate of change; γ is a multiplication factor greater than 1.0 to attain a high stiffness for unloading; and K_{in} is given by

$$K_{in} = \omega_{in} \cdot k_0 \qquad \omega_{in} = \left[1.5 \cdot (a + \sqrt{d^2 \cdot b^2 + c^2})\right]^{-4/3} \tag{27}$$

For this study, the multiplication factor γ is taken to be 4.0, which provides a sufficiently stiff unloading slope. Once the stress reaches zero, a gap δ_g is created, as shown in Fig. 5(c), and the stress will remain zero until the concrete on Side 2 assumes contact with the bar, or the bar resumes contact with the concrete on Side 1 upon reloading. The length of the gap can be calculated as

$$\delta_g = \delta_u - \frac{\sigma_u}{K_{un}} \tag{28}$$

in which σ_u and δ_u are the stress and the normal displacement at which unloading starts. For reloading toward Side 1, the stress is given by Eq. (29) until it reaches the monotonic envelope, represented by Eq. (24) and (25), and is governed by the monotonic envelope after that point.

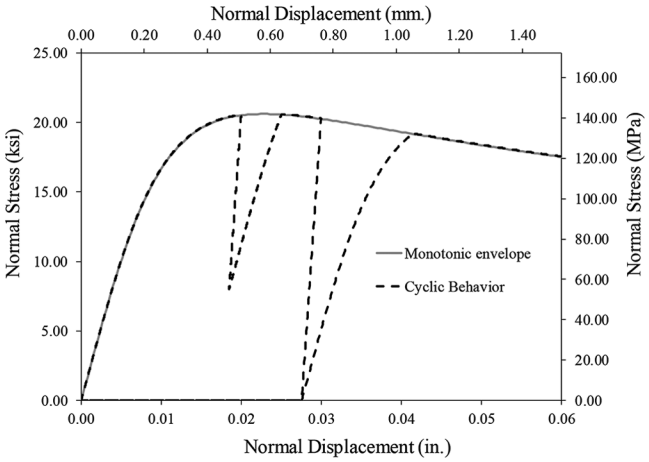

Fig. 6—Normal stress versus normal displacement curve for dowel action.

$$\sigma(\tilde{v}) = \omega(\tilde{v} - \delta_r) \cdot k_0 \left\langle \tilde{v} - \delta_r \right\rangle \tag{29}$$

In Eq. (29), $\langle \cdot \rangle$ are Macaulay brackets; the expressions for $\omega(\cdot)$ and k_0 are given in Eq. (24) and (25); and δ_r is the displacement at which reloading starts. If complete unloading occurs, δ_r is equal to δ_g, and the compressive stress will remain zero until the displacement $\tilde{v}$ reaches δ_g, at which the gap closes and the reinforcing bar resumes contact with concrete. The loading and unloading laws are illustrated in Fig. 6.

In the following sections, the bond-slip and dowel-action laws for the interface element are validated with experimental results for both monotonic and cyclic loads. The results are for bars with sufficient concrete cover so that splitting failure of concrete did not occur. The element formulation and the constitutive laws are implemented in the finite element program FEAP (Taylor 2014).

PERFORMANCE EVALUATION OF NEW INTERFACE ELEMENT

This section provides numerical examples to: 1) demonstrate that the addition of bond-slip elements can eliminate the sensitivity of numerical results to the size of the bar elements; 2) identify the optimum size of bar elements to accurately represent the bond-slip and dowel-action phenomena; 3) verify the accuracy of the new interface

element formulation in connecting concrete and bar elements with incompatible sizes; and 4) demonstrate the improved computational efficiency that can be achieved.

The physical model adopted for the numerical examples consists of two concrete blocks separated by a joint and a No. 4 steel reinforcing bar passing through the blocks, as shown in Fig. 7(a). It is modeled with plane-stress elements. In the finite element models, the nodes along the edges of the lower block are restrained from vertical and horizontal displacements, while the nodes at the edges of the upper block are subjected to uniform vertical displacements. The steel bar is modeled with beam elements. Different sizes of bar elements—namely, 1, 2, 4, and 8 in. (25, 51, 102, and 203 mm) long, are considered. The concrete elements match the size of the bar elements. Figures 7(b) and 7(c) show the coarsest and the finest meshes used in this parametric study.

The steel is modeled with a uniaxial constitutive law, which has a yield plateau and subsequent strain hardening for initial loading in one direction, and the Bauschinger effect and kinematic hardening for cyclic loading. The steel reinforcement has a Young's modulus of 29,000 ksi (200 GPa), a yield strength of 60 ksi (414 MPa), and a tensile strength of 105 ksi (724 MPa). In the interface element modeling bond slip and dowel action, the compressive strength of concrete is assumed to be 6 ksi (41 MPa). The concrete elements are represented by linearly elastic plane-stress elements with a modulus of elasticity of 4400 ksi (30 GPa).

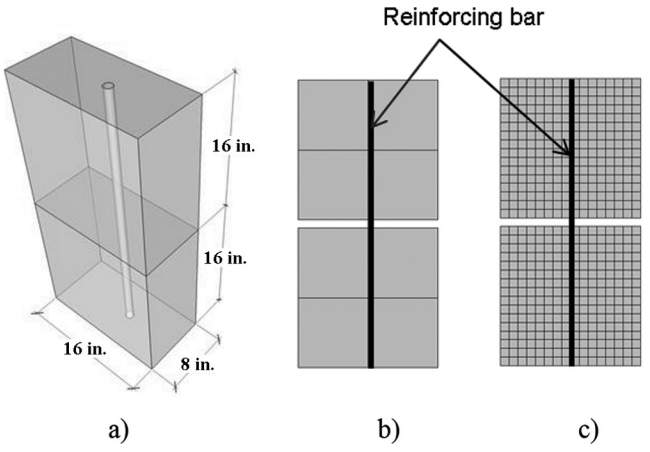

Fig. 7—Finite element models: (a) physical model; (b) coarse mesh (8 in. [203 mm] elements); and (c) fine mesh (1 in. [25 mm] elements).

To show the importance of the bond-slip elements for the objectivity of the numerical results, two analyses sets, each with different element sizes, have been conducted with the upper block subjected to an upward displacement. In the first set of analyses, no bond-slip elements are used and the bar elements are directly connected to the concrete elements, as shown in Fig. 8(a). In this case, each reinforcing bar is split into two, which are connected to the concrete elements in such a way that the connectivity is symmetric about the crack line. In the second set, bond-slip elements are used to connect the bar to the concrete, as shown in Fig. 8(b). In these analyses, the vertical forces at the nodes of the upper block are recorded and their sum is plotted against the vertical displacement.

Figure 9 shows the results for the first set of analyses. It is observed that the results are very sensitive to the element size. More specifically, the displacement at which the bar fractures and the load-displacement curves are strongly affected by the element size. This is attributed to the extent of strain localization in the bar near the joint, which is governed by the element size, as shown in Fig. 9(b). One can also notice that the results do not converge to a final solution as the element size diminishes.

Figure 10 shows the results for the second set of analyses. It can be observed that the results are only slightly affected by the element size, and the displacement at which the bar fractures converges quickly to a steady value as the element size is reduced. The sudden load drops shown in the load-

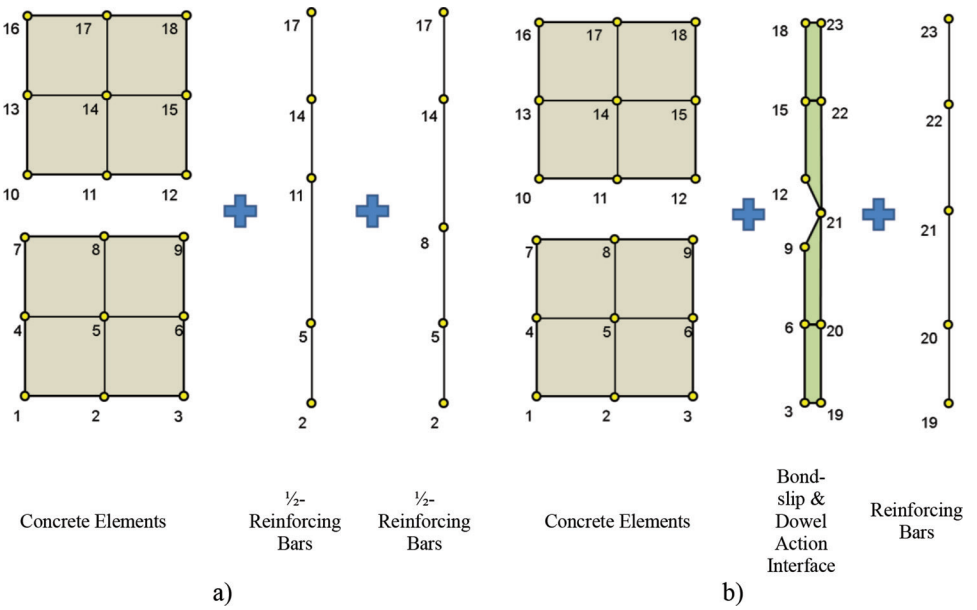

Fig. 8—Bar-concrete connectivity: (a) when no bond-slip interface elements are used; and (b) when bond-slip interface elements are used.

Table 1—Discretization information and analysis time for example problems

	No. of nodes	No. of elements				Time, s	
		Concrete	Bar	Interface	Total	Vertical displacement	Horizontal displacement
Fine mesh	611	512	32	32	576	192	435
Coarse mesh	51	8	32	32	72	20	71

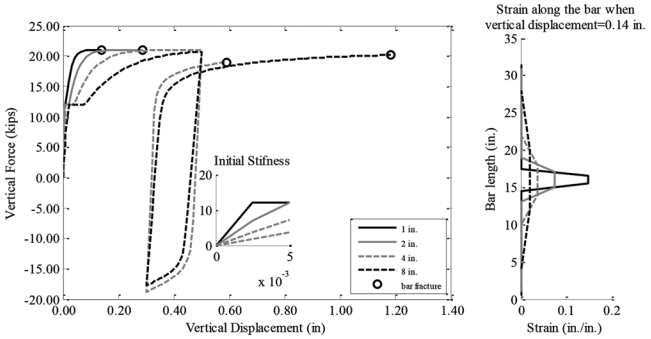

Fig. 9—Analyses without bond-slip elements: a) force-displacement; and (b) strain along bar. (Note: 1 in. = 25.4 mm; 1 kip = 4.45 kN.)

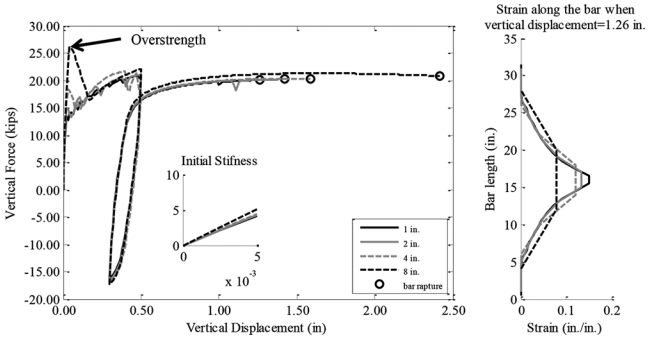

Fig. 10—Analyses with bond-slip elements: (a) force-displacement; and (b) strain along bar. (Note: 1 in. = 25.4 mm; 1 kip = 4.45 kN.)

displacement curves are due to the drops of the bond stress in the bond-slip elements. The curves become smoother as the mesh is refined because bond deterioration becomes more gradual and continuous. Moreover, as shown in Fig. 10(b), the extent of strain localization is independent of the element size even though the strain magnitude is still affected. In Fig. 10(a), the significant overstrength shown by the curve with 8 in. (203 mm) elements is because coarser mesh requires a larger bar deformation to trigger the first bond slip.

A numerical study considering different bar diameters and element sizes has indicated that the length of each bar element has to be no more than $0.5d_b$ to accurately capture the dowel action effect. In this study, a horizontal displacement is applied to the nodes at the edges of the top concrete block of Fig. 7, while the lower concrete block is prevented from moving in the horizontal direction. The total horizontal force (dowel force) is plotted against the applied horizontal displacement in Fig. 11. It can be observed that the solution converges when the element size is around $0.5d_b$. Similar analyses not reported herein have shown that to capture the bond-slip behavior, the bar elements have to be no more than

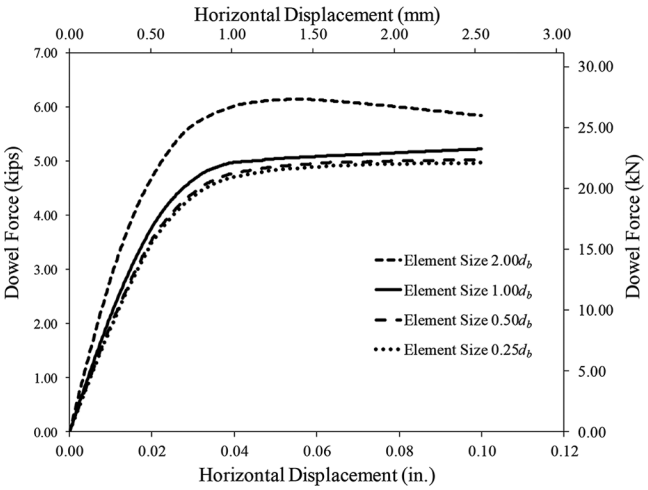

Fig. 11—Simulation of dowel action with different element sizes.

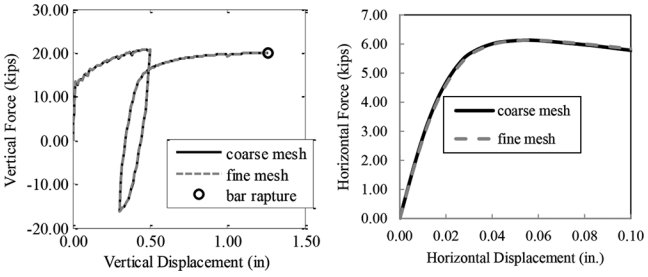

Fig. 12—Comparison of numerical results with different element sizes for concrete and the same element size for steel: (a) vertical loading; and (b) horizontal loading. (Note: 1 in. = 25.4 mm; 1 kip = 4.45 kN.)

$2.0d_b$ (Mavros 2015). Hence, the selection of the element size is governed by the dowel action.

Although a fine mesh is needed for the bar to capture the bond-slip and dowel-action mechanisms accurately, it is not required for the concrete when the bond-slip and dowel action are modeled by the proposed interface elements. This is demonstrated by using the coarse mesh and the fine mesh shown in Fig. 7(b) and Fig. 7(c) for the concrete only, while the bar elements are 1 in. (25 mm) long for both cases. Bond slip and dowel action are considered in separate analyses. The results are shown in Fig. 12(a) and 12(b), and the required computation time for each analysis is shown in Table 1. The results are not sensitive to the size of the concrete elements.

VALIDATION FOR MODELING DOWEL ACTION

Tests on single dowel bars

The ability of the constitutive law and the interface element proposed herein to simulate the dowel action of

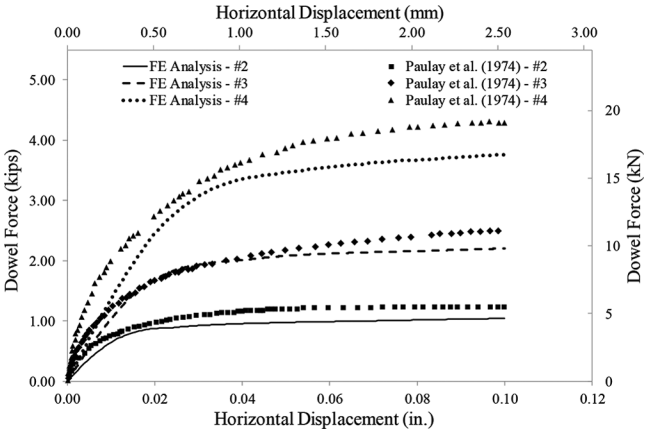

Fig. 13—Comparison of experimental and numerical results for dowel-action tests with monotonically increasing displacements ($f_c' = 3.58$ ksi [25 MPa]).

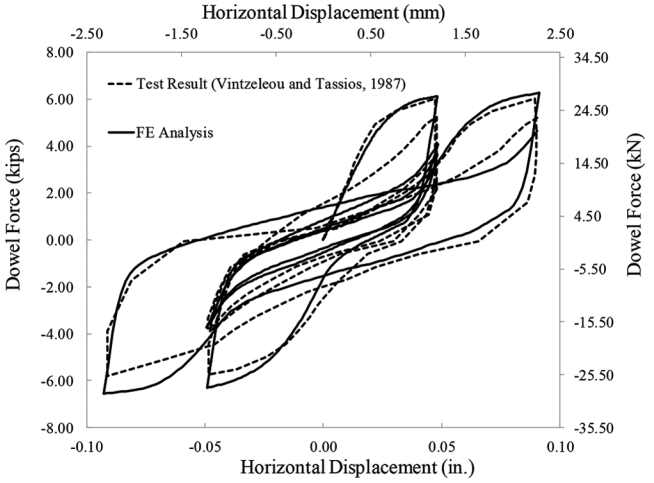

Fig. 14—Comparison of experimental and numerical results for cyclic dowel-action tests.

reinforcing bars are evaluated with the experimental data of Paulay et al. (1974), who conducted dowel tests on No. 2, No. 3, and No. 4 bars, each embedded in two concrete blocks separated by a joint, and the data from the cyclic loading tests of Vintzeleou and Tassios (1987). Paulay et al. (1974) applied melted wax to the joint between the blocks to eliminate any cohesive resistance so that the dowel resistance of the bar could be directly measured. Vintzeleou and Tassios (1987) separated the concrete blocks with 0.16 in. (4 mm) thick metal sheets, which were later removed and filled with paraffin to create a sliding plane. The concrete blocks used by Paulay et al. (1974) had an average compressive strength of 3.58 ksi (24.7 MPa), and the steel bars had yield strengths between 42.7 and 50 ksi (294 and 345 MPa). For the tests of Vintzeleou and Tassios (1987), the actual strengths of the materials were not reported. The concrete had a nominal compressive strength of 6.525 ksi (45 MPa) and the steel bars had a nominal yield strength of 61 ksi (420.5 MPa) (Vintzeleou 1984).

In the finite element analyses presented herein, beam elements are used to model the reinforcing steel bars and the proposed interface elements are used to model the dowel behavior. Concrete is modeled with linearly elastic plane-stress elements. The model used to simulate these tests has the same configuration as the one shown in Fig. 8(b). The upper concrete block is restrained from vertical displacement and is displaced horizontally. The bottom concrete block is restrained from vertical and horizontal displacements.

A bar element size of $0.25d_b$ is chosen for the analyses. Numerical results are compared to the experimental results of Paulay et al. (1974) in Fig. 13, which shows that the proposed model can capture the dowel behavior well. The discrepancies in the dowel strengths obtained from the tests and the analyses are 15%, 12%, and 12% for the No. 2, No. 3, and No. 4 bars, respectively.

The model is used to simulate the dowel behavior in the cyclic loading tests of Vintzeleou and Tassios (1987). As shown in Fig. 14, the numerical results are in good agreement with the experimental data in terms of the predicted stiffness and force capacity. In the second loading cycle, the stiffness reduction at reloading is due to the damage at the gap created between the concrete and the steel bar at the interface. The stiffness increases as the gap is being closed until further damage has been inflicted.

Analyses of shear keys in bridge abutments

The dowel-action model has been used to simulate the behavior of two shear keys in a bridge abutment model tested by Borzogzadeh et al. (2006). The shear keys considered are designated as 5A and 5B, whose reinforcement details are presented in Fig. 15. Each shear key had a construction joint separating it from the stem wall of the abutment. The stem wall had 14 No. 4 horizontal bars placed in two layers near the top as shear reinforcement, as shown in Fig. 15. The stem wall was cast before the shear keys. Shear Key 5A was constructed with a rough construction joint. A relatively thick layer of foam was placed to separate the shear key from the stem wall around the outer boundary of the joint such that the rough contact surface between the shear key and the stem wall was limited to an 8 x 8 in. (203 x 203 mm) area. Four No. 4 vertical dowel bars passed through the joint region. Shear Key 5B had a smooth construction joint. Hydraulic oil was applied to the joint to eliminate the cohesive force. Like Shear Key 5A, it had four vertical No. 4 dowel bars.

The finite element model of the shear key specimen is shown in Fig. 16. By taking advantage of the symmetry of the test specimen about the center plane of the stem wall, only a one-fourth-width slice of the specimen is modeled in the finite element analysis. Concrete is modeled with shell elements. Because the nonlinear behavior is concentrated at the construction joint and in the interfaces simulating the dowel action, the shell elements have a linearly elastic material law. The elements are 4 x 4 in. (102 x 102 mm), which allows appropriate positioning of the vertical and horizontal reinforcing bars. The shell elements are interconnected with interface elements that have the cohesive crack constitutive law proposed by Koutromanos and Shing (2011), which allow the accurate simulation of horizontal cracks and diagonal cracks, assumed to be at 45 degrees. The model can simulate crack opening and closing and horizontal sliding along a crack plane, as well as reversible shear dilatation

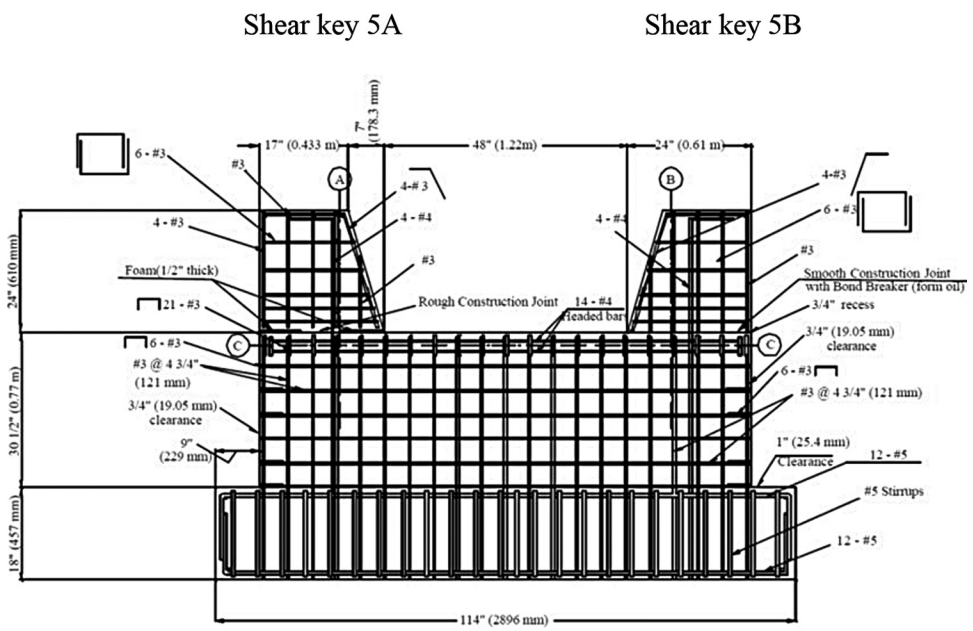

Fig. 15—Elevation view of design details for shear key specimen (from Borzogzadeh et al. [2006]).

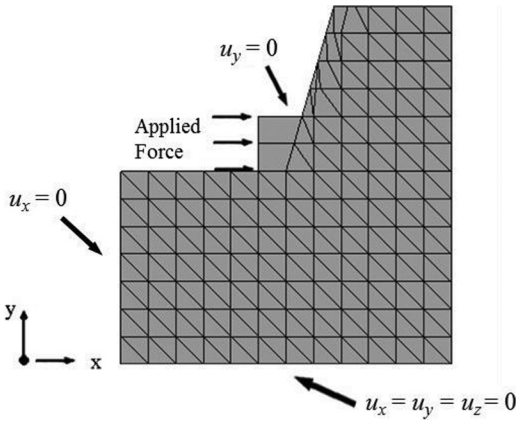

Fig. 16—Finite element model for shear key specimen and boundary conditions.

and irreversible joint compaction. It has a failure surface governing a mixed mode (Mode I and Mode II) fracture condition, and a set of softening laws governing the gradual degradation of the frictional resistance and cohesion.

To simulate the rough construction joint in Shear Key 5A, the initial coefficient of friction is assumed to be 1.0 and the cohesive strength is set to 0.87 ksi (6 MPa). The residual coefficient of friction, after significant sliding, is assumed to be 0.7. The Mode I fracture energy is assumed to be 0.0006 kip/in. (0.0001 kN/mm). The Mode II fracture energy is taken to be 10 times that of Mode I. The interface is calibrated such that significant dilatation occurs during sliding to reflect the roughness of the surface. The remaining interface elements representing the unbonded part of the construction joint have zero tensile strength and a coefficient of friction of 0.01. This small coefficient of friction is needed to avoid numerical problems in the analysis.

Shear Key 5B was completely isolated from the stem wall. Thus, all the interface elements representing the construction joint have zero tensile strength and a constant coefficient of friction of 0.36, as suggested by Borzogzadeh et al. (2006). More information for the cohesive crack interface model can be found in Koutromanos and Shing (2011).

The vertical and horizontal side reinforcing bars of the stem wall are modeled with elastoplastic truss elements that have a post-yield strain hardening slope of 2% of the initial modulus of elasticity. To simulate the dowel action, the vertical reinforcing bar crossing the construction joint of a shear key is modeled with fiber section beam elements, which are connected to the shell elements through the proposed interface element that simulates the bond-slip and dowel-action behavior. The length of the beam elements is chosen to be $0.5d_b$. The beam elements have both geometric and material nonlinearities. The constitutive model for steel developed by Dodd and Restrepo-Posada (1995) is used to describe the material nonlinearity. This model has been modified in this study to be able to capture the fracture of the dowels. Bar fracture occurs at a specified tensile strain of 20%, after which the stress decreases linearly following a slope that is 0.2% of the elastic stiffness.

The tensile strength of the vertical dowel bars is based on the values reported by Borzogzadeh et al. (2006). For the vertical dowel bars (No. 4 bars), the yield strength is 63 ksi (434 MPa) and the ultimate tensile strength is 104 ksi (717 MPa). The modulus of elasticity is equal to 29,000 ksi (200 GPa). The side reinforcement (No. 3 bars) and horizontal shear reinforcement of the stem wall have a yield strength of 68 ksi (469 MPa).

Figures 17 and 18 show that the finite element model is able to reproduce the stiffness and the strengths of both shear keys very accurately. The force-displacement curves for Shear Key 5A, as presented in Fig. 17, have the peak force occurring at a very low displacement. This peak resistance can be largely attributed to the cohesive force in the construction joint. The sudden drop of the resistance after the peak is caused by the loss of the cohesive force. Shear Key 5B did not have cohesive resistance in the construction joint due to the use of bond breaker, which is apparent in

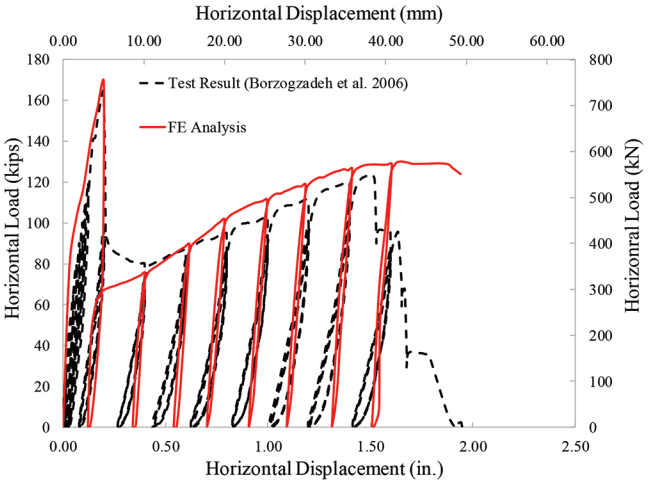

Fig. 17—Experimental and numerical results for Shear Key 5A.

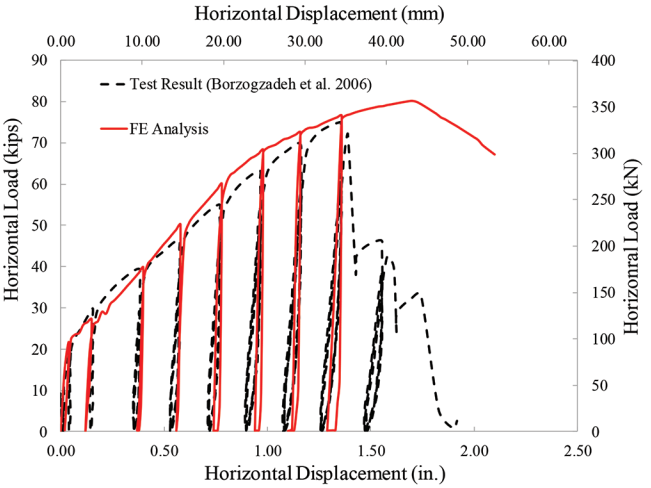

Fig. 18—Experimental and numerical results for Shear Key 5B.

the force-displacement curves in Fig. 18. However, after the load drop, Shear Key 5A has its resistance increase again as the displacement increases, showing the same behavior as 5B. This increase in resistance is due to the tension force developed in the vertical dowel bars, which lean sideway as the horizontal displacement of the shear keys increases. This phenomenon is captured by incorporating the geometric nonlinearity of the bars in the analyses. The final load drops exhibited by both shear keys are due to the fracture of the bars. In the test, Borzogzadeh et al. (2006) observed that the angle of inclination of the dowel bars with respect to the vertical at bar fracture was approximately 37 degrees. The numerical results show that this angle is approximately 34 degrees for Shear Key 5A and 35 degrees for 5B.

CONCLUSIONS

In this paper, a new interface element formulation is presented for the finite element modeling of bond slip and dowel action in reinforced concrete structures. The proposed interface model connects reinforcing bar elements to concrete elements, and has the nonlinear behavior of the concrete during bond-slip and dowel action represented in a zero-thickness interface. The novelty of the element is that it allows the reinforcing bars to be represented by a fine mesh and the concrete by a much coarser mesh, which can thus significantly improve the computational efficiency. The bond-slip and dowel-action phenomena are modeled with separate constitutive laws that account for cyclic as well as monotonically increasing loads. While the accuracy of the bond-slip law has been demonstrated in a prior publication, this study has shown that the incorporation of bond slip can avoid the localization of plastic strain in a single bar element and thus alleviate the mesh-size sensitivity issue. The accuracy of the cyclic dowel-action model and the improved computational efficiency introduced by the new interface element formulation have been demonstrated by numerical examples. Numerical results have indicated that the length of a bar element should not be more than 0.5 times the bar diameter to accurately simulate both dowel action and bond slip. However, the proposed model has limitation that the interaction between bond slip and dowel action is ignored in the constitutive laws. A constitutive model that accounts for this interaction should be developed in a future study.

AUTHOR BIOS

Alexandra Kottari *is an Engineer at Hinman Consulting Engineers Inc., San Francisco, CA. She received her BS from the National Technical University of Athens, Greece, and her MS and PhD from the University of California, San Diego (UC San Diego), La Jolla, CA. Her research interests include finite element analysis and testing of reinforced concrete structures.*

Marios Mavros *is an Engineer at Simpson Gumpertz & Heger Inc. He received his bachelor's degree from the National Technical University of Athens, and his MS and PhD from UC San Diego. His research interests include the finite element modeling and large-scale testing of masonry structures.*

ACI member **Juan Murcia-Delso** *is an Assistant Professor at the University of Texas at Austin, Austin, TX. He received his BS/MS from the Technical University of Catalonia, Barcelona, Spain, and his PhD from UC San Diego. His research interests include the nonlinear behavior and seismic performance of reinforced concrete structures.*

ACI member **P. Benson Shing** *is a Professor of Structural Engineering at UC San Diego. He received his BS, MS, and PhD from the University of California, Berkeley, Berkeley, CA. His research interests include seismic design as well as the behavior and performance of concrete and masonry structures, including large-scale testing and analytical modeling.*

ACKNOWLEDGMENTS

This study was supported by the California Department of Transportation under Contract No. 65A0424 and the National Institute of Standards and Technology under ARRA Award No. 60NANB10D013. Opinions expressed in this paper are those of the authors and do not necessarily represent those of the sponsors.

REFERENCES

Borzogzadeh, A.; Megally, S.; Restrepo-Posada, J. I.; and Ashford, S., 2006, "Capacity Evaluation of Exterior Sacrificial Shear Keys of Bridge Abutments," *Journal of Bridge Engineering*, ASCE, V. 11, No. 5, pp. 555-565. doi: 10.1061/(ASCE)1084-0702(2006)11:5(555)

Brenna, A.; Dei Poli, S.; and Di Prisco, M., 1990, "Dowel Action: Some Experimental and Theoretical Results Regarding Special Concretes," Studie Ricerche, Milan University of Technology, Milan, Italy, pp. 321-380.

Cox, J. V., and Herrmann, L. R., 1998, "Development of a Plasticity Bond Model for Steel Reinforcement," *Mechanics of Cohesive-Frictional Materials*, V. 3, No. 2, pp. 155-180. doi: 10.1002/(SICI)1099-1484(199804)3:2<155::AID-CFM45>3.0.CO;2-S

Dei Poli, S.; Di Prisco, M.; and Gambarova, P. G., 1992, "Shear Response, Deformations, and Subgrade Stiffness of a Dowel Bar Embedded in Concrete," *ACI Structural Journal*, V. 89, No. 6, Nov.-Dec., pp. 665-675.

Dodd, L. L., and Restrepo-Posada, J. I., 1995, "Model for Predicting Cyclic Behaviour of Reinforcing Steel," *Journal of Structural Engineering*, ASCE, V. 121, No. 3, pp. 433-445. doi: 10.1061/(ASCE)0733-9445(1995)121:3(433)

Dulacska, H., 1972, "Dowel Action of Reinforcement Crossing Cracks in Concrete," *ACI Journal Proceedings*, V. 69, No. 12, Dec., pp. 754-757.

Fédération Internationale du Béton (fib), 2000, "Bond of Reinforcement in Concrete," *fib Bulletin 10*, Lausanne, Switzerland, 434 pp.

Koutromanos, I., and Shing, P. B., 2011, "Cohesive Crack Model to Simulate Cyclic Response of Concrete and Masonry Structures," *ACI Structural Journal*, V. 109, No. 3, May-June, pp. 349-358.

Mavros, M., 2015, "Experimental and Numerical Investigation of the Seismic Performance of Reinforced Masonry Structures," PhD thesis, University of California, San Diego, La Jolla, CA, 216 pp.

Murcia-Delso, J., and Shing, P. B., 2015, "Bond-Slip Model for Detailed Finite-Element Analysis of Reinforced Concrete Structures," *Journal of Structural Engineering*, ASCE, V. 141, No. 4, p. 04014125 doi: 10.1061/(ASCE)ST.1943-541X.0001070

Paulay, T.; Park, R.; and Philips, M. H., 1974, "Horizontal Construction Joints in Cast in Place Reinforced Concrete," *Shear in Reinforced Concrete*, SP-42, American Concrete Institute, Farmington Hills, MI, pp. 599-616.

Soroushian, P.; Obaseki, K.; and Rojas, M. C., 1987, "Bearing Strength and Stiffness if Concrete Under Reinforcing Bars," *ACI Materials Journal*, V. 84, No. 3, May-June, pp. 179-184.

Taylor, R. L., 2014, "FEAP – Finite Element Analysis Program," University of California, Berkeley, Berkeley, CA, http://www.ce.berkeley.edu/feap. (last accessed June 1, 2017)

Van Mier, J. G. M., and Van Vliet, M. R. A., 2003, "Influence of Microstructure of Concrete on Size/Scale Effects in Tensile Fracture," *Engineering Fracture Mechanics*, V. 70, No. 16, pp. 2281-2306. doi: 10.1016/S0013-7944(02)00222-9

Vintzeleou, E., 1984, "Mechanisms of Load Transfer Along Reinforced Concrete Interfaces Under Monotonic and Cyclic Actions," PhD thesis, Department of Civil Engineering, National Technical University of Athens, Athens, Greece, 549 pp.

Vintzeleou, E., and Tassios, T. P., 1987, "Behavior of Dowels Under Cyclic Deformations," *ACI Structural Journal*, V. 84, No. 1, Jan.-Feb., pp. 18-30.